Single-cycle powerful megawatt to gigawatt terahertz pulse radiated from a wavelength-scale plasma oscillator

Hui-Chun Wu,[1,2,*] Zheng-Ming Sheng,[1,3,†] and Jie Zhang[1,3]
[1]*Beijing National Laboratory of Condensed Matter Physics, Institute of Physics, Chinese Academy of Science, Beijing 100080, China*
[2]*Max-Planck-Institut für Quantenoptik, D-85748 Garching, Germany*
[3]*Department of Physics, Shanghai Jiaotong University, Shanghai 200240, China*
(Received 12 November 2007; revised manuscript received 12 February 2008; published 15 April 2008)

We propose a scheme to generate single-cycle powerful terahertz (THz) pulses by ultrashort intense laser pulses obliquely incident on an underdense plasma slab of a few THz wavelengths in thickness. THz waves are radiated from a transient net current driven by the laser ponderomotive force in the plasma slab. Analysis and particle-in-cell simulations show that such a THz source is capable of providing power of megawatts to gigawatts, field strength of MV/cm–GV/cm, and broad tunability range, which is potentially useful for nonlinear and high-field THz science and applications.

DOI: 10.1103/PhysRevE.77.046405 PACS number(s): 52.25.Os, 42.65.Re, 42.72.Ai, 52.59.Ye

I. INTRODUCTION

Terahertz (THz) spectroscopy can probe spectral properties of molecules in a previously inaccessible electromagnetic spectrum [1]. Its applications include the characterization of semiconductors [2] and high-temperature superconductors [3], THz imaging of biomedical tissues [4], cellular structures [5], and dielectric substances [6], and manipulation of bound atoms [7]. Most applications are based on the techniques of THz time-domain spectroscopy (TDS) [1], which employs coherent broadband (2–5 THz bandwidth) THz pulses. Nowadays, most broadband pulsed THz sources are based on the excitation of different materials with ultrashort laser pulses [1], such as through photoconduction or optical rectification, but the output power is limited by the damage threshold of the materials used.

Recently, by four-wave mixing [8–11] or ionization-induced transient currents [12] in air with laser intensities of $10^{14}-10^{15}$ W/cm^2, single-cycle THz pulses with field strength on the order of kV/cm have been produced. For light intensities $I \gg 10^{15}$ W/cm^2, the leading part of the laser pulse can completely ionize the material and the interaction process becomes a pure laser-plasma interaction. Plasma has no thermal damage threshold and can sustain extremely intense light. The peak intensity of lasers today can be as high as 10^{20} W/cm^2 and in the future is expected to reach 10^{23} W/cm^2 [13]. New THz emission mechanisms in the context of intense laser-plasma interactions may produce higher-power THz sources.

A possible THz emission source is based on the generation of a laser wakefield, an electron plasma wave driven by the laser ponderomotive force $F_p=-mc^2/(2\gamma)\nabla a_L^2$ [14], where m is the electron rest mass, c is the light velocity in vacuum, γ is the electron relativistic factor, and $a_L=eA_L/mc$ is the normalized laser vector potential, which is related to the light intensity through $I=a_L^2\times 1.37\times 10^{18}$ $(\mu\mathrm{m}/\lambda)^2$ W/cm^2; here λ is the laser wavelength in vacuum. The relativistic laser intensity is reached for $a_0 \geq 1$. The laser wakefield at a small amplitude in a uniform plasma is described by $\delta n=\delta n_p \exp[i(k_p x-\omega_p t)]$, where δn_p is the electron density perturbation; $\omega_p=\sqrt{ne^2/m\varepsilon_0}=5.64\times 10^4$ $(n/\mathrm{cm}^{-3})^{1/2}$ Hz is the background plasma (with density n) frequency, $-e$ is the electron charge; and $k_p=\omega_p/c=2\pi/\lambda_p$, where λ_p is the plasma wavelength. For the underdense plasma with $n<n_c$, ω_p can fall in the THz region, e.g., $n=10^{16}$ cm^{-3}, $\omega_p/2\pi=0.9$ THz. Here $n_c=m\varepsilon_0\omega^2/e^2=1.1\times 10^{21}$ $(\mu\mathrm{m}/\lambda)^2$ cm^{-3} is the critical density, beyond which the laser cannot propagate, and ω is the laser angular frequency. This infinite one-dimensional (1D) plasma wave can never emit electromagnetic waves at frequency $\omega_p/2\pi$ (or wavelength λ_p), since its displacement current $(\varepsilon_0\partial\mathbf{E}_w/\partial t)$ exactly compensates for the plasma current $(-en\mathbf{v})$. This means that the wakefield is a pure electrostatic wave. However, it is found that wakefields in a magnetized plasma [15] or nonuniform plasma [16–19] can emit THz waves through Cerenkov radiation or linear mode conversion mechanisms. Both mechanisms have a plasma length $L \gg \lambda_p$ and the generated THz pulses are in multicycles.

The present work introduces a rather simple THz emission scheme based on the laser wakefield, which can uniquely generate a single-cycle THz pulse in the context of laser-plasma interaction. This is realized by exciting a laser wakefield in a plasma slab with the length $L \sim \lambda_p$. THz waves are radiated from a transient net current driven by the laser ponderomotive force. Analysis and particle-in-cell (PIC) simulations show that such a THz source is capable of providing power of megawatts to gigawatts, field strength of MV/cm–GV/cm, and broad tunability range.

In Sec. II we explain this THz emission mechanism and deduce an analytic scaling of the THz field amplitude as a function of laser intensity, incident angle, and plasma density. In Sec. III we give 1D PIC simulation results and confirm the analytic scaling. To illustrate multidimensional properties of THz emissions, some two-dimensional (2D) PIC simulation results are presented in Sec. IV. Finally, in Sec. V, we discuss the effects of nonuniform plasmas and laser duration, the limit of this THz emission mechanism, and some practical considerations.

*hui-chun.wu@mpq.mpg.de
†zmsheng@aphy.iphy.ac.cn

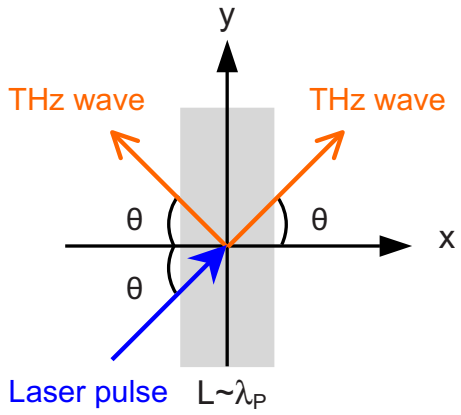

FIG. 1. (Color online) Schematic of THz emission from a plasma oscillator excited by a laser pulse obliquely incident on a few-wavelength uniform plasma slab. The plasma length is $L \sim \lambda_p$ and θ is the laser incident angle. THz waves are radiated in both specular reflection and transmission directions.

II. THz EMISSION MECHANISM FROM A PLASMA OSCILLATOR AND ANALYTIC MODEL

A limited wakefield with $L \sim \lambda_p$ (called a plasma oscillator) can radiate electromagnetic waves for the following straightforward reasons. First, for such a few-plasma-wavelength plasma oscillator, its displacement current and real current cannot completely counteract each other. Second, the plasma skin depth of the radiation at frequency ω_p is simply k_p^{-1}, which is comparable to the plasma length L. Therefore the radiation can tunnel through the thin plasma layer into vacuum. Figure 1 shows a schematic of this THz emission mechanism.

In the following we give a theoretical analysis of this THz emission mechanism. For the interaction geometry shown in Fig. 1, by Lorentz transformations, we transform all the physical quantities from the laboratory frame to a moving frame with velocity $c \sin \theta \mathbf{e}_y$, where $\mathbf{e}_y$ is the unit vector along the y direction. Electromagnetic waves with $\omega^L = \omega'$ and $\mathbf{k}^L = (\pm k' \cos \theta, k' \sin \theta, 0)$ in the laboratory frame become $\omega^M = \omega' \cos \theta$ and $\mathbf{k}^M = (\pm k' \cos \theta, 0, 0)$ in the moving frame, wherein all the electromagnetic waves propagate along the $\pm x$ directions. So THz emissions in the laboratory frame must be in the specular reflection and laser transmission directions. Plasma (electrons and ions) in the moving frame streams along $-\mathbf{e}_y$, with a relativistic factor $\gamma^M = 1/\cos \theta$. Following Ref. [20] and using the quasistatic approximation [21], we obtain the coupled equations (in SI units)

$$\left(\frac{\partial^2}{\partial x^2} - \frac{1}{c^2} \frac{\partial^2}{\partial t^2} \right) \mathbf{a}_T = \frac{\omega_p^2}{c^2} \mathbf{s}(x,t), \tag{1}$$

$$\frac{\partial^2 \phi}{\partial x^2} = \frac{\omega_p^2}{c^2} \delta n, \tag{2}$$

$$\delta n = \frac{1}{2 \cos \theta} \left(\frac{1 + (\mathbf{a}_L - \mathbf{e}_y \tan \theta)^2}{(1/\cos \theta + \phi)} - 1 \right), \tag{3}$$

where $\mathbf{s}(x,t) = -\delta n \tan \theta \mathbf{e}_y / \gamma$ is the THz radiation source, $\mathbf{a}_T$ and $\mathbf{a}_L$ are, respectively, the vector potentials of the THz wave and incident laser normalized by mc/e, ϕ is the scalar potential of the driven plasma wave normalized by mc^2/e, δn is the density perturbation of the plasma wave normalized by the initial plasma density n, $\gamma = \sqrt{1 + (\mathbf{a}_L - \tan \theta \mathbf{e}_y)^2 + p_x^2}$ is the electron relativistic factor, and p_x is the electron longitudinal momentum normalized by mc. In deducing Eq. (1), the direct current and THz nonlinear terms have been omitted.

THz radiation is determined by Eq. (1), from which the electric field in the laboratory frame is found to be [20]

$$\mathbf{e}_T^L(x,t) = \frac{\omega_p}{2\omega \cos \theta} \int_0^L \frac{dx'}{k_p^{-1}} \mathbf{s}(x', t - |x - x'|/c), \tag{4}$$

where L is the plasma length, and normalization with respect to $m\omega c/e = 3.2 \times 10^4 \ (\mu\text{m}/\lambda)$ MV/cm has been performed. In the weakly relativistic approximation $\phi \ll 1$ (i.e., $a_L < 1$), Eqs. (2) and (3) lead to $\delta n \propto a_L^2 \cos \theta$. In the THz emission process, we assume $\gamma \simeq \gamma^M$. Substituting these into Eq. (4), one obtains

$$\mathbf{e}_T^L \propto C n^{1/2} a_L^2 \sin \theta \mathbf{e}_y, \tag{5}$$

under the limit $L \sim \lambda_p$. Here the plasma density n is normalized by the critical density n_c; the constant C depends on the laser pulse shape and plasma density distribution and will be determined from particle-in-cell simulations. Because the wakefield itself is in the xy interaction plane, THz emission is always p polarized. The emission field amplitude is proportional to $n^{1/2} a_L^2$, due to the laser-driven wakefield amplitude $E_w \propto \omega_p a_L^2$ [14,17]. Equation (5) also predicts that the emission field increases monotonically with $\sin \theta$ for $\theta < 90°$. Physically, this can be attributed to the fact that the emission source area is increased when the incident angle is increased. There is no THz emission for normal incidence $\theta = 0°$, since there is no transverse wakefield component.

The 1D analytic scaling Eq. (5) and 1D PIC simulations in the next section are valid as long as the laser spot size is large compared with the plasma wavelength and the laser intensity is uniform in the laser focus. For a laser beam with a Gaussian profile $\exp(-r^2/w_L^2)$ in transverse space, the 1D model applies for $w_L \gg \lambda_p$. For $w_L < \lambda_p$, the radiation source size is smaller than the radiated wavelength, so that the generated THz wave will diffract dramatically, as shown by 2D PIC simulations in Sec. IV. In order to have collimated THz emission, it is necessary to have $w_L > \lambda_p$.

III. 1D PIC SIMULATIONS

To test our proposal and the scaling rule Eq. (5), we conduct a series of 1D and 2D PIC simulations. Taking into account the oblique incidence of the laser beam, our 1D PIC code adopts a moving frame as discussed above [20,22] and outputs all physical quantities in the laboratory frame. The incident laser pulse has a sine-squared profile $a_L = eA_L/mc = a_0 \sin^2[\pi(x - ct)/d_L]$ for $0 \le x - ct \le d_L$, where d_L is the laser pulse duration. The laser pulse enters the left boundary of the simulation box with s polarization in order to distinguish it easily from the p-polarized THz emission. For the sine-squared laser pulse, the excited wakefield amplitude reaches the maximum when $d_L \approx \lambda_p$ [17,18]. The simulation results

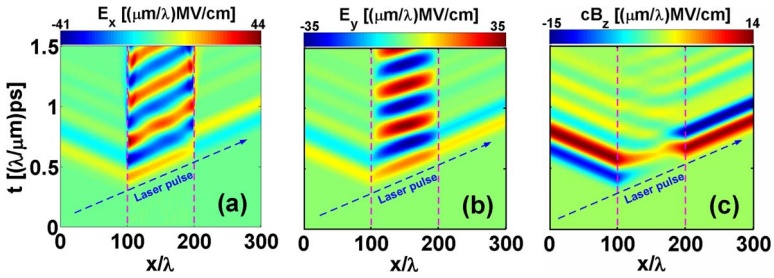

FIG. 2. (Color online) Spatial-temporal plots of the electric fields E_x (a), E_y (b), and the pure THz magnetic field B_z (c). The plasma is of density $n=0.0001n_c$ and length $L=100\lambda$ located in the $100\lambda \le x \le 200\lambda$ region. The laser pulse parameters are $a_0=0.5$, $d_L=100\lambda$, and $\theta=45°$.

also confirm that the THz emission is strongest for $d_L=\lambda_p$; thus we always set $d_L=\lambda_p$ in the following. We retain a free parameter λ in the presentation of simulation results, so that one can scale to any laser wavelength. To simplify the following discussions, we set the laser wavelength $\lambda=1$ μm.

Figure 2 plots the temporal evolution of field components E_x, E_y, and B_z in the x space. The initial plasma density is taken to be $n=0.0001n_c$. For $\lambda=1$ μm, $n=1.1\times10^{17}$ cm^{-3}. The corresponding plasma frequency is $\omega_p/2\pi=2.98$ THz, which represents the central frequency of the THz emission. The plasma wavelength is $\lambda_p=\sqrt{n_c/n}\lambda=100\lambda$. The plasma is of length $L=100\lambda$ located in the $100\lambda \le x \le 200\lambda$ region. The vertical dashed lines represent the initial plasma boundaries. The laser pulse parameters are $a_0=0.5$, $d_L=100\lambda$, and $\theta=45°$. The laser intensity is $I\approx3.4\times10^{17}$ W/cm^2. The dashed arrow marks the laser propagation trajectory. The fields E_x and E_y in Figs. 2(a) and 2(b) include the longitudinal fields of the wakefield and the electric fields of the p-polarized THz emission. The wakefield is completely localized in the plasma region, while the electric field of the THz wave is mainly outside the plasma slab. In Fig. 2(c) B_z is the pure magnetic field of the THz wave. It is obvious that two single-cycle THz pulses are radiated from the plasma region. Due to the propagation delay of the laser pulse, the pulse in the backward (reflection) direction is generated earlier than that in the forward (transmission) direction.

Defining fields $F_\pm=(E_y \pm cB_z)/2$ in the moving frame, we see that F_+ and F_- represent the forward and backward p-polarized electromagnetic waves, respectively. Tracing F_+ and F_- at the right and left boundaries of the simulation box, we can obtain the temporal profiles of the radiated THz pulses in the reflection and transmission directions. Figure 3 shows the peak field strengths $|F_\pm|_{\max}$ of the THz pulses as a function of the initial plasma length L. Other parameters are the same as in Fig. 2. The THz field strengths are found to be

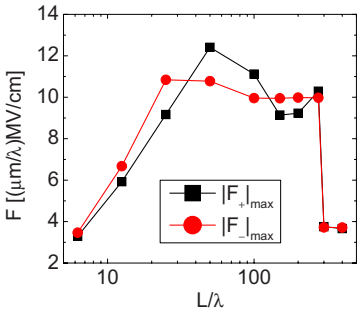

FIG. 3. (Color online) Peak field strengths $|F_\pm|_{\max}$ of the THz pulses as a function of the plasma length L.

above 10 MV/cm. To generate intense THz pulses, the plasma length L should be within $[0.25\lambda_p, 2.7\lambda_p]$ according to Fig. 3. When $L \ge 3\lambda_p$, we find that THz amplitudes decrease dramatically and the THz pulses are no longer single cycle.

Figures 4(a) and 4(b) illustrate the temporal profiles of the THz pulses shown in Fig. 2, together with another two incident angles of 30° and 60°. The shape of the transmitted THz wave F_+ is the same as that of the reflected F_-. For $\theta=30°$, the THz pulses have two cycles. Single-cycle THz emission is produced when $\theta \ge 45°$. With increasing incident angles, the number of cycles included in the THz pulse decreases. Figure 4(c) displays the power spectra of the THz pulses F_-. The central frequency is about 2.93 THz. The spectrum width increases with the incident angle, because of the shorter THz duration for the larger θ. The bandwidths approach 3–6 THz, meeting the requirements for the THz TDS system. Figure 4(d) shows that the peak field strengths $|F_\pm|_{\max}$ are proportional to $\sin\theta$, which well agrees with Eq. (5) obtained from our analytical model. There is no THz emission for $\theta=0$. We emphasize that our 2D PIC simulations (see the parameters in Sec. IV and the simulation geometry given in Fig. 7) further confirm the scaling law of Eq. (5) with the incident angles up to 75°, as shown in Fig. 4(d). These simulations suggest that the emission source area is increased when the incident angle is increased, which results in increased THz amplitudes. Different positions in the emission area emit at different times. As a whole, the THz pulses produced can still be single cycle.

Figures 5(a) and 5(b) show that THz field strengths are proportional to both the laser intensity (from 10^{14} to 10^{18} W/cm^2) and the square root of the plasma density n, as predicted by Eq. (5). In Sec. II we obtain the scaling under the weakly relativistic approximation $a_0<1$, so it is exact for the laser intensity $I<10^{18}$ W/cm^2. For $a_0>1$, the wakefield amplitude is proportional to a_0 [23], so the THz amplitude increase slowly with the laser intensity, as shown in Fig. 5(a).

According to the above results, we find $C\approx0.18$ in Eq. (5) and rewrite it in the practical form

$$e_T = 5.8n^{1/2}a_0^2 \sin\theta \ (\mu m/\lambda)\text{GV/cm}, \quad a_0 < 1. \qquad (6)$$

In the lower-intensity regime (10^{14}–10^{15} W/cm^2), the THz field strength is tens of kV/cm, comparable to that generated through four-wave mixing [8–11] or ionization-induced transient currents [12] in air. For the case with the laser intensity at 3.4×10^{17} W/cm^2 as in Fig. 2, the THz field strength approaches 10 MV/cm, i.e., an intensity of 1.3×10^{11} W/cm^2. Assuming a radiation source radius of

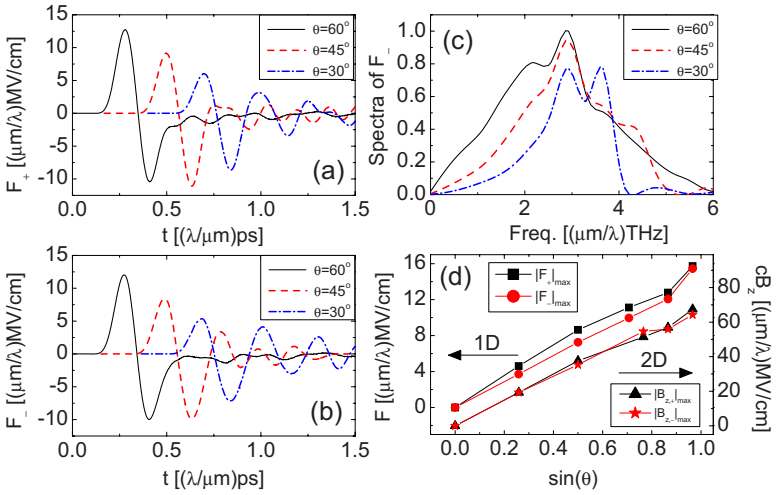

FIG. 4. (Color online) (a) Temporal profiles of the THz waves F_+ for incident angles of $\theta=30°$, 45°, and 60°. (b) Temporal profiles of the THz waves F_-. (c) Power spectra (arb. units) of F_- in (b). (d) Peak field strengths $|F_\pm|_{\max}$ of the THz pulses as a function of $\sin\theta$ with $\theta\in[0°,15°,30°,45°,60°,75°]$. 2D PIC results (see parameters in Sec. IV) are also included.

100 μm, the deduced THz power is 41 MW. The present THz emission mechanism works well at higher laser intensities. For example, for $I=3.4\times10^{19}$ W/cm^2 ($a_0=5$) and $I=1.37\times10^{20}$ W/cm^2 ($a_0=10$), our simulation results suggest that the THz field strengths can be 0.33 and 0.5 GV/cm, and the corresponding powers are about 45 and 102 GW, respectively. For these extremely intense lasers, the emitted THz pulses still are single cycle (0.33 ps duration) and pulse energies can be larger than 10 mJ.

Figure 6 shows the conversion efficiency of THz emission as a function of the laser intensity. The efficiency is proportional to the laser intensity when $I<10^{18}$ W/cm^2, and reaches more than 10^{-5} when $I\simeq10^{19}$ W/cm^2.

IV. 2D PIC SIMULATIONS

To illustrate the multidimensional properties of the THz emission, we conduct 2D PIC simulations. To save simulation time, we take $n=0.0025n_c$, corresponding to $\lambda_p=20\lambda$ and $\omega_p/2\pi=14.9$ THz. The plasma length is $L=25\lambda$. As shown in Fig. 7, the simulation box is $250\lambda\times250\lambda$, and the plasma is located in the dashed rectangular region. The laser pulse is s polarized, focused on the plasma slab surface along $y=100\lambda$, and has parameters $a_0=0.5$, $d_L=20\lambda$, and $\theta=50°$. Figure 7 shows THz magnetic fields B_z for laser radius $w_L=10\lambda$, 30λ, and 60λ at the time $t=230\lambda/c$. It is found that there are indeed two single-cycle THz pulses in the reflection and transmission directions (marked by dashed arrows). In Fig. 7(a), the fronts of the emitted THz pulses are curved. This is because the incident laser beam spot size (or the THz source size) is smaller than the THz wavelength, so that strong diffraction appears when the THz pulses propagate. Also, the tightly focused laser beam contains the wave components in different incident directions, which leads to the emission complexity. When the laser spot size is increased as in Fig. 7(b), the diffraction effect is reduced. The THz field strength reaches 42 MV/cm, i.e., an intensity of 2.5×10^{12} W/cm^2. Since the radiation radius is about 30 μm, this is equivalent to a peak power of 70 MW. Compared with Fig. 7(a), the THz pulses in Fig. 7(c) are cleaner for a larger laser spot size. Figure 8 plots the temporal profiles of THz pulses traced on the position $(x,y)=(200\lambda,100\lambda)$. The diffraction of the THz emission decreases with increasing laser radius, and the case $w_L=60\lambda$ is close to the 1D result and agrees well with the scaling Eq. (6). The dependence of THz amplitude on the incident angles given in Fig. 4(d) is obtained for the case $w_L=60\lambda$.

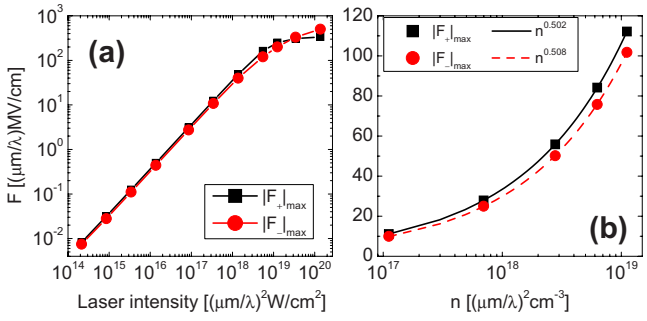

FIG. 5. (Color online) (a) Peak field strengths $|F_\pm|_{\max}$ of the THz pulses as a function of the laser intensity. We take $L=50\lambda$ and other parameters the same as in Fig. 2. (b) $|F_\pm|_{\max}$ of the THz pulses as a function of the electron density n. The laser pulse parameters are $a_0=0.5$ and $\theta=45°$. For a given plasma density n, we always take $L=d_L=\lambda_p$. The dashed lines are fitted curves.

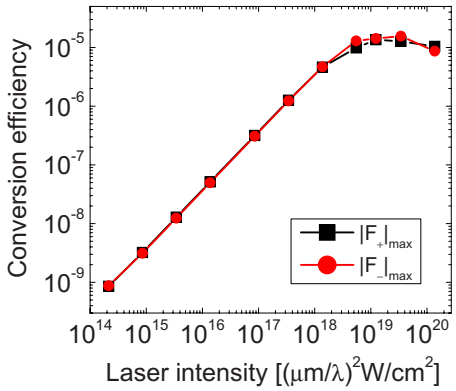

FIG. 6. (Color online) Conversion efficiency of THz emissions as a function of the laser intensity. All parameters are the same as in Fig. 5(a).

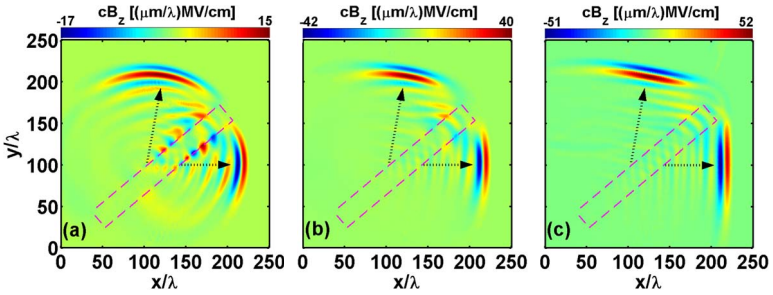

FIG. 7. (Color online) 2D spatial plot of the pure THz magnetic field B_z for $w_L=10\lambda$ (a), 30λ (b), and 60λ (c) at the time $t=230\lambda/c$ in 2D PIC simulations. The dashed arrows present the THz emission directions, one along the laser propagation and the other along the specular reflection direction.

V. DISCUSSION AND CONCLUSIONS

In the previous sections, we consider THz emission from a uniform plasma slab with sharp boundaries. In real situations, usually one obtains a nonuniform plasma slab. Now we show the effect of plasma density inhomogeneity on THz emissions through 1D PIC simulations. Figure 9 shows two density profiles of uniform and nonuniform plasmas. The uniform plasma has $L=50\lambda$. The nonuniform plasma has a trapezoid profile and is totally 150λ long. The temporal profiles and spectra of THz pulses in both reflection and transmission directions are illustrated in Fig. 10. One can see that the backward THz pulse in the nonuniform case is stronger than the uniform one [see Fig. 10(a)] and the THz central frequency is shifted to be lower for the nonuniform plasma [see Fig. 10(c)]. This is because the left plasma slope in Fig. 9 also contributes to the backward THz emission in the lower-frequency region by a kind of mode conversion [17,18] and leads to stronger THz emission. In reverse, as shown in Fig. 10(b), the forward THz pulse in the nonuniform case is weaker than the uniform one. This is because the forward p-polarized THz wave may be partially absorbed in the right plasma slope through resonant absorption [24]. As a result, only high-frequency components remain in the forward THz pulse [see Fig. 10(c)]. The reason that the right plasma slope does not emit a THz wave is that the wakefield in the descending plasma profile cannot be phase matched with the electromagnetic wave [17,18]. For the nonuniform plasma slopes with the scale much larger than λ_p, mode conversion theory [17,18] can be utilized. In this case, the emitted THz pulses are no longer single cycle and an optimal incident angle exists for the strongest backward THz emission, which is different from the scaling of Eq. (5) or Eq. (6).

The scaling Eq. (6) also can include the effect of laser duration. For the sine-squared pulse $a_0 \sin^2[\pi(x-ct)/d_L]$, the wakefield amplitude at a given plasma density (corresponding to ω_p) is $E_w=(m\omega_p c/e)(a_0^2/4)\sin(\pi d_L/\lambda_p)\{[1-(d_L/\lambda_p)^2]^{-1}-0.25[1-0.25(d_L/\lambda_p)^2]^{-1}\}$ [17,18], which is maximum with $E_{w,\max}=0.39a_0^2(m\omega_p c/e)$ at $d_L=1.1\lambda_p$. The scaling Eq. (6) is for the optimum pulse duration $d_L=\lambda_p$, so the effect of laser duration can be included in Eq. (6) by multiplying it with the factor $E_w/E_{w,\max}$.

A favorable target for the present THz emission mechanism to work is a gas jet working in a vacuum chamber, as commonly used in high-harmonic generation experiments [25]. For the desired THz region of 0.1–10 THz (wavelength 30 μm–3 mm), plasma densities and lengths need to be controlled within 10^{14}–10^{18} cm^{-3} and 30 μm–3 mm, respectively. The usual gas jet meets most of these parameters. The possible difficulty is generation of sub-100-μm gas jets for waves of 10 THz. According to Fig. 3, the plasma length also can be 75 μm for strong emission. In addition, the laser machining technique [26] can possibly be used to generate a gas jet with sub-100-μm thickness. Therefore, the gas jet may allow this THz emission to be tuned in the region of 0.1–10 THz by simply adjusting the gas density.

Finally, we discuss the limits of this THz emission mechanism. As discussed in Sec. III, THz emission amplitudes increase slowly and tend to saturate for the laser intensity $I>10^{18}$ W/cm^2. This THz emission mechanism will not work when the laser pulse is so strong as to push all electrons out of the plasma slab against the separated-charge potential;

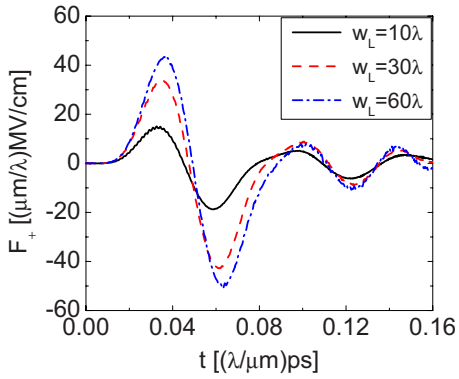

FIG. 8. (Color online) Temporal profiles of the THz waves F_+ traced on the position $(x,y)=(200\lambda,100\lambda)$ in 2D PIC simulations.

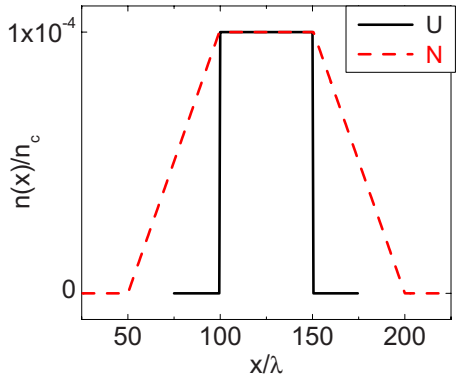

FIG. 9. (Color online) Density profiles for uniform plasma (u) with $L=50\lambda$ and nonuniform plasma (n) with a trapezoidal profile. Linear slopes are 50λ long, and the whole nonuniform plasma length is 150λ. The laser pulse parameters are the same as in Fig. 2.

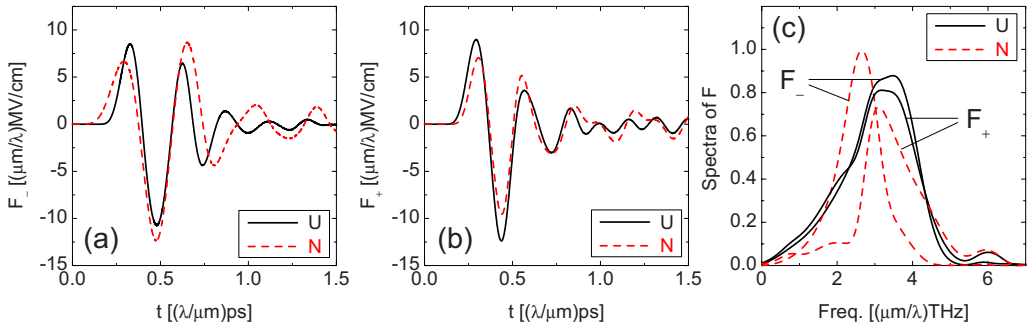

FIG. 10. (Color online) (a) Temporal profiles of the THz waves F_- for uniform (u) and nonuniform (n) plasmas. (b) Temporal profiles of the THz waves F_+. (c) Power spectra (arb. units) of F_- and F_+.

the electrons can no longer be restored and radiate electromagnetic waves. Simulations show that this extreme case occurs at $a_0 \approx 40$ (or $I > 10^{21}$ W/cm^2).

To conclude, we have presented a scheme for producing single-cycle MW–GW THz radiation from wavelength-scale ($L \sim \lambda_p$) plasma oscillators. The radiation is emitted by the transient net currents induced in the plasma slab while the plasma oscillators are built up. This scheme provides the possibility to produce coherent high-field THz radiation on the table top for applications in nonlinear and high-field THz science. Moreover, this THz emission mechanism together with that for THz emission by linear mode conversion in inhomogeneous plasmas ($L \gg \lambda_p$) [17,18] provide a complete picture of laser wakefield emission, and should be helpful for interpreting the early experimental observation of THz emission in intense laser-plasma interactions [27].

ACKNOWLEDGMENTS

The authors are grateful to Professor L.-A. Wu for careful reading of the manuscript, and to Dr. Y. Cang for useful discussions. This work was supported by the NSFC (Grant Nos. 10425416 and 10390160), the National High-Tech ICF Committee in China, the Knowledge Innovation Program, CAS, and the National Basic Research Program of China (Grant No. 2007CB310406). H.C.W. acknowledges support from the Alexander von Humboldt Foundation.

[1] B. Ferguson and X.-C. Zhang, Nat. Mater. **1**, 26 (2002).
[2] D. Grischkowsky, S. Keiding, M. van Exter, and C. Fattinger, J. Opt. Soc. Am. B **7**, 2006 (1990).
[3] R. A. Kaindl, M. A. Carnahan, J. Orenstein, D. S. Chemla, H. M. Christen, H.-Y. Zhai, M. Paranthaman, and D. H. Lowndes, Phys. Rev. Lett. **88**, 027003 (2001).
[4] T. Lőffler, T. Bauer, K. Siebert, H. Roskos, A. Fitzgerald, and S. Czasch, Opt. Express **9**, 616 (2001).
[5] O. Mitrofanov, M. Lee, J. W. P. Hsu, I. Brener, R. Harel, J. F. Federici, J. D. Wynn, L. N. Pfeiffer, and K. W. West, IEEE J. Sel. Top. Quantum Electron. **7**, 600 (2001).
[6] B. Ferguson, S. Wang, D. Gray, D. Abbott, and X.-C. Zhang, Opt. Lett. **27**, 1312 (2002).
[7] B. E. Cole, J. B. Williams, B. T. King, M. S. Sherwin, and C. R. Stanley, Nature (London) **410**, 60 (2001).
[8] D. J. Cook and R. M. Hochstrasser, Opt. Lett. **25**, 1210 (2000).
[9] M. Kress, T. Lőffler, S. Eden, M. Thomson, and H. G. Roskos, Opt. Lett. **29**, 1120 (2004).
[10] T. Bartel, P. Gaal, K. Reimann, M. Woerner, and T. Elsaesser, Opt. Lett. **30**, 2805 (2005).
[11] X. Xie, J. Dai, and X.-C. Zhang, Phys. Rev. Lett. **96**, 075005 (2006).
[12] K. Y. Kim, J. H. Glownia, A. J. Taylor, and G. Rodriguez, Opt. Express **15**, 4577 (2007).
[13] G. A. Mourou, T. Tajima, and S. V. Bulanov, Rev. Mod. Phys. **78**, 309 (2006).
[14] E. Esarey, P. Sprangle, J. Krall, and A. Ting, IEEE Trans. Plasma Sci. **PS-24**, 252 (1996).
[15] J. Yoshii, C. H. Lai, T. Katsouleas, C. Joshi, and W. B. Mori, Phys. Rev. Lett. **79**, 4194 (1997).
[16] Z.-M. Sheng, H.-C. Wu, K. Li, and J. Zhang, Phys. Rev. E **69**, 025401(R) (2004).
[17] Z.-M. Sheng, K. Mima, J. Zhang, and H. Sanuki, Phys. Rev. Lett. **94**, 095003 (2005).
[18] Z.-M. Sheng, K. Mima, and J. Zhang, Phys. Plasmas **12**, 123103 (2005).
[19] H.-C. Wu, Z.-M. Sheng, Q.-L. Dong, H. Xu, and J. Zhang, Phys. Rev. E **75**, 016407 (2007).
[20] R. Lichters, J. Meyer-ter-Vehn, and A. Pukhov, Phys. Plasmas **3**, 3425 (1996).
[21] P. Sprangle, E. Esarey, and A. Ting, Phys. Rev. A **41**, 4463 (1990).
[22] A. Bourdier, Phys. Fluids **26**, 1804 (1983).
[23] W. Lu, M. Tzoufras, C. Joshi, F. S. Tsung, W. B. Mori, J. Vieira, R. A. Fonseca, and L. O. Silva, Phys. Rev. ST Accel. Beams **10**, 061301 (2007).
[24] W. L. Kruer, *The Physics of Laser Plasma Interactions* (Addison-Wesley, Redwood City, CA, 1988), Chap. 4, p. 39.
[25] Ch. Spielmann, N. H. Burnett, S. Sartania, R. Koppitsch, M. Schnűrer, C. Kan, M. Lenzner, P. Wobrauschek, and F. Krausz, Science **278**, 661 (1997).
[26] C.-T. Hsieh, C.-M. Huang, C.-L. Chang, Y.-C. Ho, Y.-S. Chen, J.-Y. Lin, J. Wang, and S.-Y. Chen, Phys. Rev. Lett. **96**, 095001 (2006).
[27] H. Hamster, A. Sullivan, S. Gordon, W. White, and R. W. Falcone, Phys. Rev. Lett. **71**, 2725 (1993).